SUPPLEMENTARY INFORMATION

Supp. Table 1 provide the years of the EP-El Niño and the CP-El Niño during DJF for each decade from the 1870s using the SST with and without a linear trend. Note that both the EP-El Niño and the CP-El Niño was not observed before the 1870s and the winter of 1870 indicates D(1870)JF(1871). The total occurrence number of EP-El Niño is 31 and that of CP-El Niño is 7 using the detrended SST. There are subtle differences of the EP-El Niño years and the CP-El Niño years whether the SST data is detrended or not. For instance, the EP-El Niño years after 1990 are 1991, 1997, 2003 and 2006 based on the detrended SST data, on the other hand, those are 1991, 1997, 2002, 2003, and 2006 based on the non-detrended SST data. Using the detrended SST data, for the period of 1854-2007, the occurrence ratio of the EP-El Niño before and after 1990 is 0.20/year and 0.23/year, respectively, while that of the CP-El Niño before and after 1990 is 0.01/year and 0.29/year, respectively. Similar to the results based on the non-detrended SST data, the frequency of CP-El Niño occurrence has been remarkably increased during recent decades. One may argue that there is a distinct absence of SST data in the Pacific Ocean prior to 1930. Therefore, we apply the same procedure to the SST data after 1930 (Supp. Table 2). For the period of 1930-2007, the frequency of EP-El Niño before and after 1990 is unchanged (0.23/year), while that of CP-El Niño before and after 1990 is 0.05/year and 0.35/year, respectively. Such a tendency is also detectable even if the data is detrended for the same period (Supp. Table 2). Furthermore, we analyzed the SST taken from the Hadley Centre[1] for the period of 1870-2007 and from the Kaplan extended SST version 2[2] for the period of 1856-2007. Supp. Table 3 displays the frequency of EP-El Niño and CP-El Niño before and after 1990 in both different datasets of SST. We reach to similar result that the CP-El Niño is more frequently observed after 1990.

Supp. Fig. 1 shows an 11-year window sliding correlation coefficients between the DJF NINO3 SST index and the DJF NINO4 SST index for the period of 1870-2006. Strikingly, the relationship between the two NINO indices gradually decreases during recent decades. Substantial reduction in the 11-year sliding correlation coefficients is observed after 1990 when the CP-El Niño frequently occurred. This result indicates that the NINO4 SST index becomes more independent on the NINO3 SST index in recent decades. The maximum correlation coefficient is 0.99 for the period of 1892~1902 (i.e., 11 years) and the minimum correlation coefficient is 0.71 for the period of 1995~2005. In spite of that, one may argue that the NINO4 SST index, which is used to define the CP-El Niño in this study, is quantitatively different from that for the canonical El Niño. To ensure this, we calculate a simultaneous correlation coefficient between the DJF NINO4 SST index and DJF El Niño Modoki Index[3] for the period of 1979-2006. The correlation coefficient is significantly high, 0.79, in contrast, the correlation between the DJF NINO3 SST index and DJF El Niño Modoki Index is very low 0.27. Simply put, this result indicates that the index for the CP-El Niño can grasp the different flavor of El Niño compared to the conventional El Niño as in the recent studies.

Supp. Table 4 summarizes the description of the selected eleven CGCM simulations. The CGCM simulations are made available by the Program for Climate Model Diagnosis and Intercomparison (PCMDI) at web site http://www-pcmdi.llnl.gov/ipcc/about_ipcc.php and detailed descriptions of 20C3M and SRESA1B run are found. We chose the eleven CGCMs because these CGCMs are available for the data for the simulation period of 100 years after the concentration of CO2 is fixed to about 700 ppm.

Supp. Fig. 2a,b show the ensemble mean composite of the EP-El Niño and the CP-El Niño during winter in the 20C3M run, respectively. Supp. Figs. 2c,d are the same as in Supp. Figs. 2a,b except for the SRESA1B run. Similar to the observations, we define the EP-El Niño and the CP-El Niño using the NINO3 and the NINO4 SST indices during winter in the 20C3M run and the SRESA1B run, respectively. Compared to the observations, the EP-El Niño simulated in the 20C3M run (Supp. Fig. 2a) is similar except a westward expansion. Such discrepancies are also observed in the simulated CP-El Niño in the 20C3M run (Supp. Fig. 2b), that is to say, the center of maximum SST is shifted to the west compared to the observations. From the 20C3M run (Supp. Figs. 2a,b) to the SRESA1B run (Supp. Figs. 2c,d), the maximum amplitude of anomalous SST in both EP-El Niño and the CP-El Niño is slightly reduced, however, the spatial pattern of the two types of El Niño is little changed. We also provide the ensemble mean composite of the EP-El Niño and the CP-El Niño during summer in the 20C3M run and the SRESA1B run (Supp. Fig. 3). The westward migration of maximum anomalous SST is readily apparent from summer (Supp. Fig. 3a) to winter (Supp. Fig. 2a) in the EP-El Niño in the 20C3M run. In contrast, there is little indication of the CP-El Niño from summer (Supp. Fig. 3c) to winter (Supp. Fig. 2c). The prominent structure in the CP-El Niño during summer (Supp. Fig. 3c) in which anomalous warm SST is confined within the western and central equatorial Pacific is quite similar to that during winter (Supp. Fig. 2c). This indicates that the CP-El Niño is trapped in the western and central equatorial Pacific during its seasonal evolution, which is comparable to the observations[4]. Such characteristics are also seen in the CP-El Niño in the SRESA1B run (Supp. Fig. 2d and Fig. 3d), however, the westward migration of maximum anomalous SST in the EP-El Niño in the SRESA1B run is relatively weak compared to that in the 20C3M run.

The occurrence ratio of CP-El Niño/EP-El Niño is around 0.2 in the observations (Supp. Table 1), which is much smaller than that in the ensemble mean ratio of CP-El Niño/EP-El Niño in the 20C3M run in the eleven CGCMs (0.97). That is to say, the CGCMs tend to simulate more frequently the CP-El Niño events compared to observation. This is because the El Niño simulated in the CGCMs is shifted to the west presumably due to the common cold bias over cold tongue region[5]. In spite of this, we obtain the result that change in El Niño statistics due to climate change projection may be characterized by more frequent occurrence of the CP-El Niño compared to the EP-El Niño. For example, we compare the occurrence ratio of CP-El Niño/EP-El Niño between the observations and the 20C3M run in the period of 1900-1999. Among eleven CGCMs, we select six CGCMs in which the occurrence ratio of CP-El Niño/EP-El Niño is close to the observations, i.e., CNRM-CM3, FGOALS-g1.0, MRI-CGCM2.3.2, PCM, UKMO-HadCM3 and UKMO-HadGEM1. The ensemble mean ratio of CP-El Niño/EP-El Niño for those six CGCMs in the 20C3M run is 0.31. In addition, those six CGCMs reasonably simulate the amplitude ratio of NINO4 SST index/NINO3 SST index in comparison with the observations. The occurrence ratio of CP-El Niño/EP-El Niño increases from the 20C3M run to the SRESA1B run in five CGCMs (See Fig. 3). The ensemble mean ratio of CP-El Niño/EP-El Niño in the SRESA1B run for the six CGCMs is 1.53, which increases as much as five times compared to the 20C3M run (0.31). Note that the ensemble mean ratio of CP-El Niño/EP-El Niño in the SRESA1B run for the eleven CGCMs is 1.67, which increases as much as 70% compared to the 20C3M run (0.97).

There may exist other sources for the El Niño evolution towards more frequent occurrence of CP-El Niño during recent decades. For instance, recent study[3] have argued

that the observed intensification in the CP-El Niño activity is primarily driven by strengthening of the interaction between intraseasonal variability in the equatorial Pacific and ENSO under global warming. In addition, there is an argument that the intraseasonal variability plays an important role on the recent occurrence of El Niño Modoki[3,6]. It is difficult to address this issue in the multi-model ensemble considering that for most models, only the monthly mean outputs are available, which limits the investigation of the intraseasonal variability. Note that it is likely that global warming also impacts the intraseasonal variability which in turn can rectify ENSO, which makes it a difficult issue to tackle with. Nevertheless, we provide a diagnosis on the change in thermocline depth in the multi-models (Fig. 4) because it is the parameter that impacts in a straight forward manner the ENSO variability and as so, provide preliminary material for the physical interpretation of the statistical results. These changes are interpreted in the light of simple considerations based on current ENSO theory and recent studies that focus on equatorial dynamics. Further studies are required to address this issue in a more comprehensive manner.

Supp. Fig. 4 illustrates how the El Niño pattern changes from the 20C3M run to the SRESA1B run in the UKMO-HadCM3 model whose occurrence ratio in the CP-El Niño/EP-El Niño increases the largest among the CGCMs and that has similar CP-El Niño/EP-El Niño ratio as in the observations. Supp. Fig. 4 shows the SSTA variability during winter in the 20C3M run (Supp. Fig. 3a) and the SRESA1B run (Supp. Fig. 4b) in UKMO-HadCM3 model, respectively. The maximum value of SSTA variability in the SRESA1B run reaches approximately 1.6°C, which is not much different from that in the 20C3M run. However, it is clear that the center of maximum SSTA variability is shifted to

the west from the 20C3M run to the SRESA1B run, which can be seen in the zonal structure of the SSTA variability averaged in 2°N-2°S (Supp. Fig. 4c).

Supp. Figs. 5a,b show the difference of ensemble mean composite for the anomalous atmospheric circulation at 500hPa between the CP-El Niño and the EP-El Niño (i.e., CP-El Niño minus EP-El Niño) in the 20C3M run and the SRESA1B run, respectively. Large differences are found in the centers of action in the atmosphere over the central and eastern North Pacific between the two different types of El Niño in both the 20C3M run (Supp. Fig. 5a) and the SRESA1B run (Supp. Fig. 5b). From the 20C3M run to the SRESA1B run, such differences are enhanced, with in particular an eastward shift of the dipole like pattern of Fig. 3d.

Reference

1. Rayner, N. A., Parker, D. E., Horton, E. B., Folland, C. K., Alexander, L. V., Rowell, D. P., Kent, E. C., & Kaplan, A. Global analyses of sea surface temperature, sea ice, and night marine air temperature since the late nineteenth century. *J. Geophy. Res*. **108**, D14, 4407, 10.1029/2002JD002670 (2003).

2. Kaplan, A., Cane, M., Kushnir, Y., Clement, A., Blumenthal, M., & Rajagopalan, B. Analyses of global sea surface temperature 1856-1991. *J. Geophy. Res.* **103**, 18,567-18,589 (2001).

3. Ashok , K., Behera, S. K., Rao, S. A., Weng, H. & Yamagata, T. El Niño Modoki and its possible teleconnection. *J. Geophy. Res*. **112**, C11007, doi:10.1029/2006JC003798 (2007).

4. Kug, J.-S., Jin, F.-F., & An, S.-I. Two types of El Niño events: Cold tongue El Niño and Warm pool El Niño. *J. Climate*, **22**, 1499-1515 (2009).

5. Capotondi, A., Wittenberg, A., & Masina, S. Spatial and temporal structure of tropical Pacific interannual variability in 20th century coupled simulations. *Ocean Modelling*, **15**, 274-298 (2006).

6. McPhaden, M., Zebiak, S. E., & Glantz, M. H. ENSO as an integrating concept in Earth Science. *Science*, **314**, 1740 (2006).

Supp. Table 1 The EP-El Niño and CP-El Niño years using the raw SST and detrended SST for each decade from 1854, respectively.

	Raw SST		Detrended SST	
	EP-El Niño years	CP-El Niño years	EP-El Niño years	CP-El Niño years
1850s				
1860s				
1870s	1876, 1877		1876, 1877	
1880s	1888		1888	
1890s	1896, 1899		1896, 1899	
1990s	1902,1904,1905		1902,1904,1905	
1910s	1911,1913,1914		1911,1913,1914,1918	
1920s	1925		1925	
1930s	1930, 1939		1930, 1939	
1940s	1940,1941		1940,1941	
1950s	1951,1957		1951,1957	
1960s	1963,1965,1969	1968	1963,1965,1969	1968
1970s	1972,1976,1979	1977	1972,1976,1979	1977
1980s	1982,1986,1987		1982,1986,1987	
1990s	1991,1997	1990,1992,1994	1991,1997	1990, 1994
2000s	2002,2003,2006	2001,2004	2003,2006	2001,2002,2004

Supp. Table 2 The EP-El Niño and CP-El Niño years using the raw SST and detrended SST for each decade from 1930, respectively.

	Raw SST		Detrended SST	
	EP-El Niño years	CP-El Niño years	EP-El Niño years	CP-El Niño years
1930s	1930,1939		1930,1939	
1940s	1940,1941		1940,1941	
1950s	1951,1957		1951,1957	
1960s	1963,1965,1969	1968	1963,1965,1969	1968
1970s	1972,1976	1977,1979	1972,1976,1979	1977
1980s	1982,1986,1987		1982,1986,1987	
1990s	1991,1997	1990,1992,1994	1991,1997	1990,1994
2000s	2003,2006	2001,2002,2004	2006.	2002,2004

Supp. Table. 3. The frequency of EP-El Niño and CP-El Niño in the SST from the Hadley Centre and the Kaplan extended SST version2.

SST dataset	El Niño type	Frequency	
		Before 1990	After 1990
The SST from the Hadley Centre	EP-El Niño	0.21/year	0.11/year
	CP-El Niño	0.05/year	0.41/year
The SST from the Kaplan extended SST version 2	EP-El Niño	0.23/year	0.17/year
	CP-El Niño	0.08/year	0.35/year

Supp. Table 4 The CGCM analyzed in this study.

Model name (Center, country)	Global oceanic resolution (Longitude× Latitude)	Simulation period	
		20C3M	SRES A1B
CGCM3_1 (T47) (CCCMA, Canada)	192×96	151 years	300 years
CNRM-CM3 (CNRM, France)	180×170	140 years	300 years
GFDL_CM2_0 (NOAA GFDL, USA)	360×200	140 years	300 years
GFDL_CM2_1 (NOAA GFDL, USA)	360×200	140 years	300 years
FGOALS-g1.0 (IAP, China)	360×170	150 years	200 years
INM-CM3.0 (INM, Russia)	144×84	130 years	200 years
MIROC3_2_medres (CCSR/NIES, Japan)	256×192	151 years	300 years
MRI_CGCM2_3_2a (MRI, Japan)	144×111	150 years	300 years
PCM (NCAR, USA)	360×180	110 years	300 years
UKMO-HadCM3 (Hadley Center, UK)	288×144	140 years	200 years
UKMO-HadGEM1 (Hadley Center, UK)	360×216	200 years	200 years

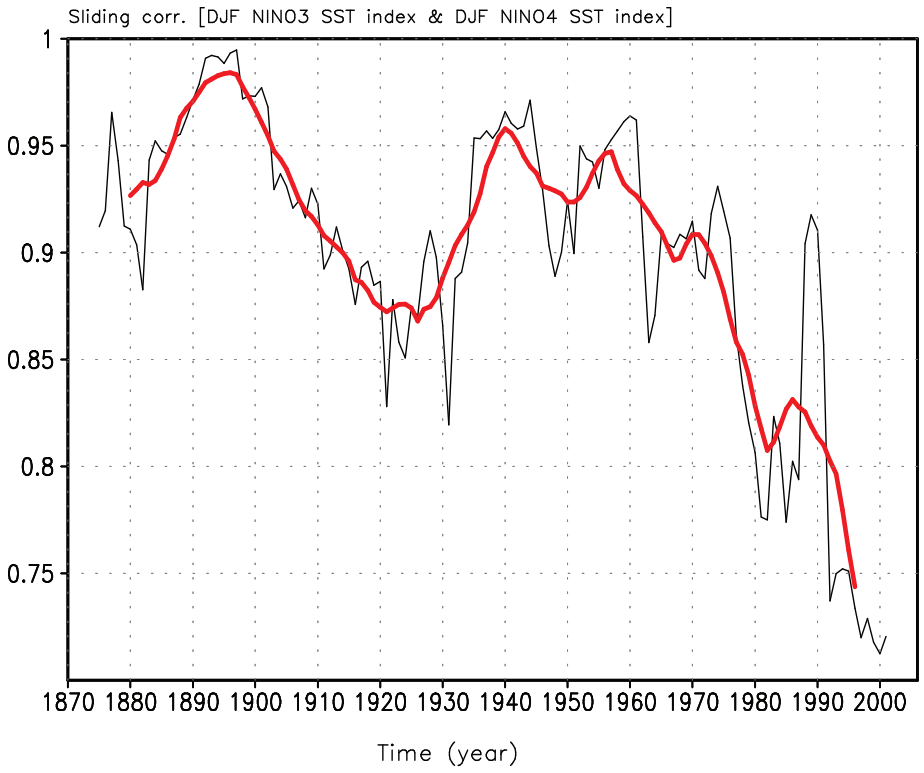

Supp. Figure 1 11-year window sliding correlation coefficients between the DJF NINO3 SST index and the DJF NINO4 SST index for the period of 1870-2006 (black). Red line indicates an 11-year running mean time series.

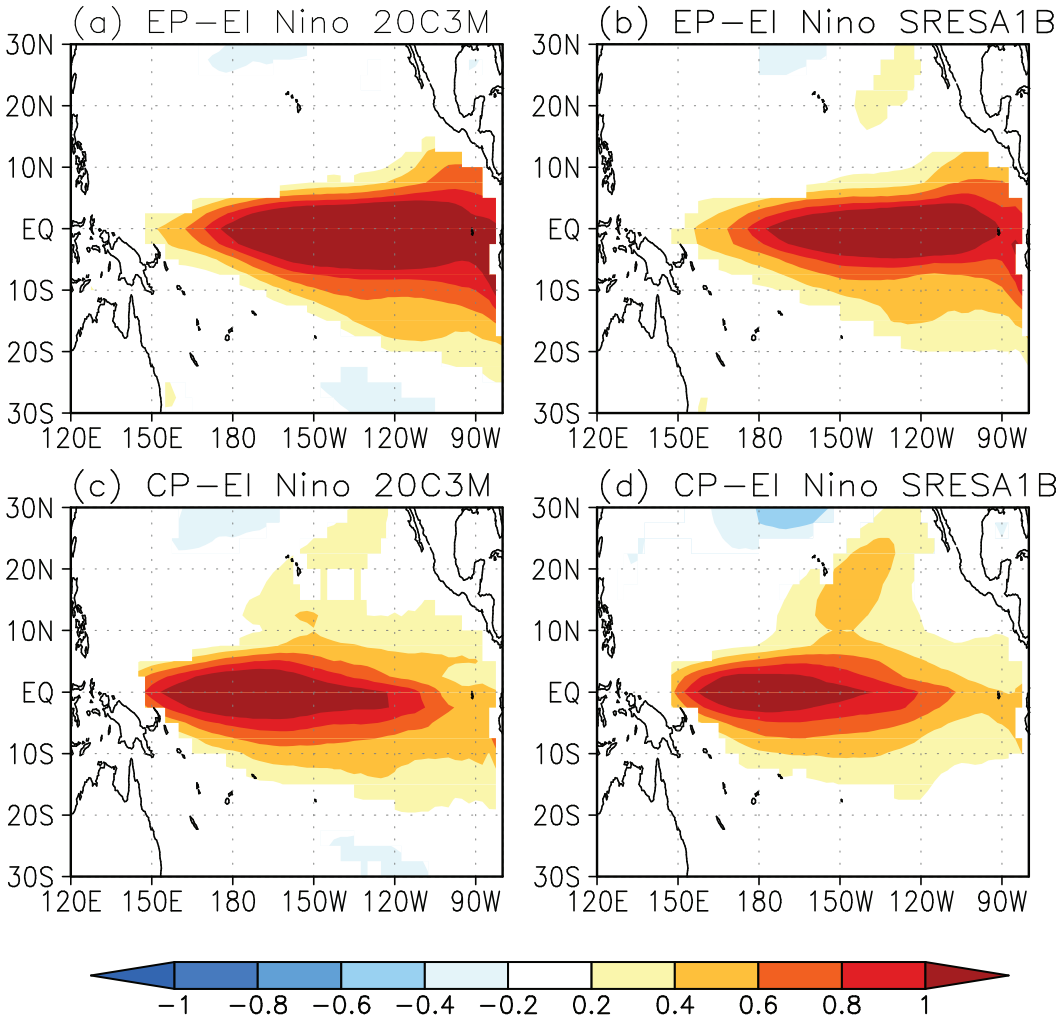

Supp. Figure 2 The composite of anomalous mean SST for the EP-El Niño (a) and the CP-El Niño (b) during the boreal winter in the 20C3M run. (c), (d) are the same as in (a), (b) except for the SRESA1B run. Shading denotes a statistical significance at 95% confidence level.

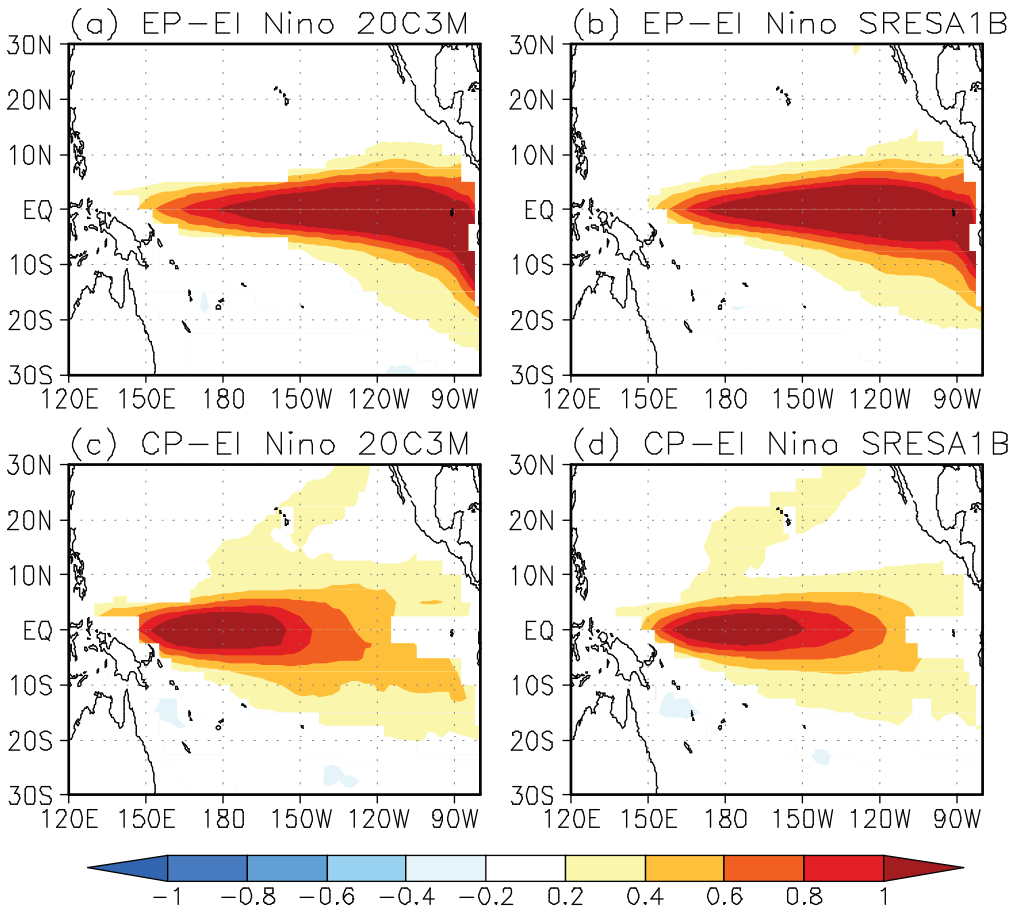

Supp. Figure 3 Supp. Fig. 3 is the same as in Supp. Fig. 2 except for the EP-El Niño and the CP-El Niño during the boreal summer.

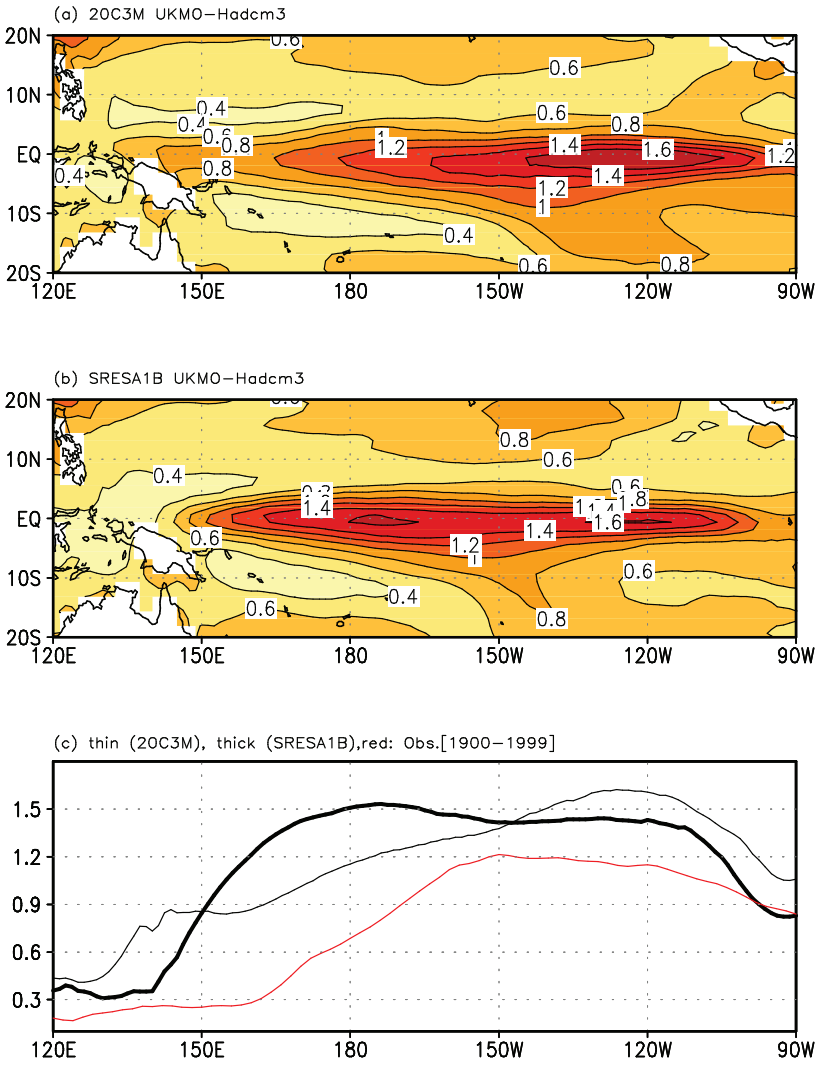

Supp. Figure 4. The standard deviation of SSTA variability during winter in the UKMO-HadCM3 in the 20C3M run (a) and that in the SRESA1B run (b). Contour interval is 0.2°C. (c) is the zonal structure of the standard deviation of SSTA variability averaged over 2°N-2°S in the 20C3M run (thin), the SRESA1B run (thick), and the observations (red line) for the period of 1900-1999 during winter, respectively.

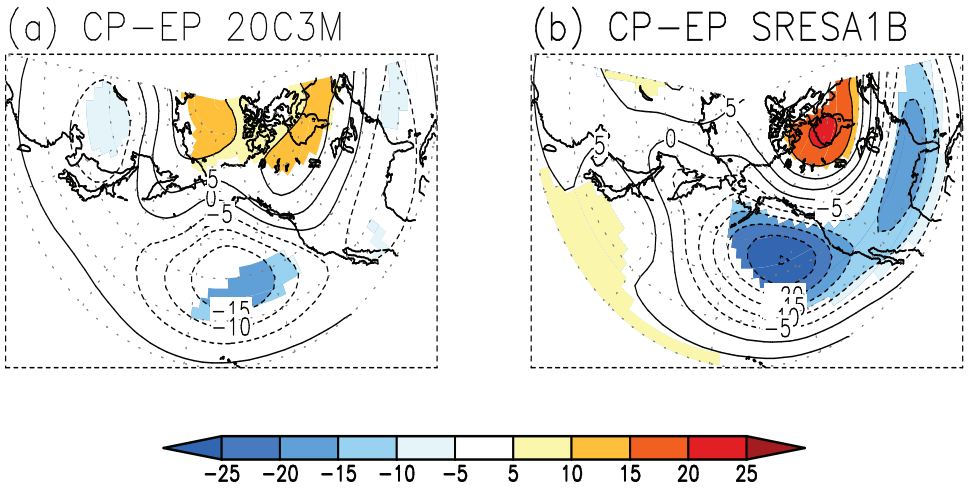

Supp. Figure 5 The difference of ensemble mean composite for the anomalous atmospheric circulation at 500hPa between the CP-El Niño and the EP-El Niño (i.e., CP-El Niño minus EP-El Niño) in the 20C3M run (a) and the SRESA1B run (b), respectively. Contour interval is 5m. The ensemble mean is formed from the nine CGCMs which provide the 500hPa geopotential height data: CCCma CGCM3.1(T47), CNRM-CM3, GFDL-CM2.0, GFDL-CM2.1, FGOALS-g1.0, MIROC3.2(medres), MRI-CGCM2.3.2, PCM, and UKMO-HadCM3. Shading denotes a statistical confidence at 95% confidence level.